Stanford Exploration Project, Report 84, May 9, 2001, pages 1–151

Amplitude-preserved processing and analysis of the Mobil AVO data set[1]

David E. Lumley, Dave Nichols[2], Christine Ecker,
Thorbjørn Rekdal[3] and Arnaud Berlioux

ABSTRACT

Mobil Oil has released a comprehensive seismic and well-log data set from the North Sea to benchmark AVO techniques. We present our results on amplitude-preserved data processing and analysis of the Mobil AVO data. First, we apply a source and receiver consistent amplitude balancing to the seismic data, which reduces source and receiver amplitude variance from about 8% and 15% respectively, to within a few percent scatter. Next, we apply a time-domain conjugate-gradient multiple-suppression technique to remove multiple reflection energy and simultaneously preserve and enhance primary-reflection AVO amplitudes. We perform unmigrated AVO analyses and find that the multiple-suppressed data correlate better with the well-log data than the unprocessed data. A prestack migration/inversion of the multiple-suppressed data shows a clear improvement over unmigrated AVO analysis, and reveals an undrilled graben block in the center of the line that exhibits a positive hydrocarbon indicator anomaly.

INTRODUCTION

Mobil Oil has released a comprehensive seismic and well-log data set as an open benchmark of AVO techniques. We initially found that the data were so heavily contaminated with multiple reflections (water-column peglegs), that it would be nearly impossible to perform a reasonable AVO analysis without first removing multiples. However, this must be done in a manner which simultaneously preserves the primary AVO response. This led directly to a new method for amplitude-preserved multiple suppression developed by Lumley, Nichols and Rekdal (1995). We believe this method to be a new practical tool useful for suppressing multiple reflections without compromising subsequent AVO analysis. We were also surprised to find that raw source and receiver consistent amplitude variations were as high as 10% and 20% respectively. These source-receiver amplitude variations cause undesirable scatter in AVO amplitude analysis, and can smear any attempt at amplitude-preserved multiple suppression or prestack migration. This led Lumley and Berlioux to develop a quick and robust method for estimating and applying the necessary source-receiver amplitude corrections. We demonstrate the effects of amplitude balancing, multiple suppression, conventional unmigrated AVO analysis, and a prestack migration/inversion method. We show a distinct improvement in the quality of AVO

[1] A modified version of this paper was presented at a 1994 SEG Workshop in Los Angeles, and has been submitted for publication in a special SEG Workshop Proceedings.

[2] Currently at Geco-Prakla, Gatwick, UK.

[3] Currently at PGS Seres, Oslo, Norway.

information after multiple suppression, and in comparing prestack migration/inversion results to conventional unmigrated AVO analysis.

AMPLITUDE BALANCING

Amplitude variations

Figure **??** is a display of trace rms-amplitude as a function of shot position and offset. The trace amplitude is calculated in a triangular-tapered window on each trace from 5-6 seconds record time, after geometric spreading and NMO corrections. The late time of this window helps to suppress the effects of source-receiver directivity since most reflection energy is propagating near-vertical at all offsets. It also avoids spatially-variable reflection signal biasing the trace amplitude estimate since most energy is incoherent noise at these late arrival times. The dark vertical stripes in Figure **??** correspond to missing shots in the data set. Each horizontal band corresponds to a single hydrophone group (receiver) in the marine cable, and the grayscale value shows the variable amplitude sensitivity of receivers along the cable. For example, the two adjacent dark gray horizontal stripes at about 1 km offset represent two hydrophone groups which are relatively weak compared to other receiver groups. The overall amplitude variations are on the order of 10–20% of the average amplitude in the plane, and may cause undesirable systematic scatter in any amplitude-preserved processing step or AVO analysis. Shot and receiver consistent amplitude balancing is required to suppress this undesirable amplitude contamination.

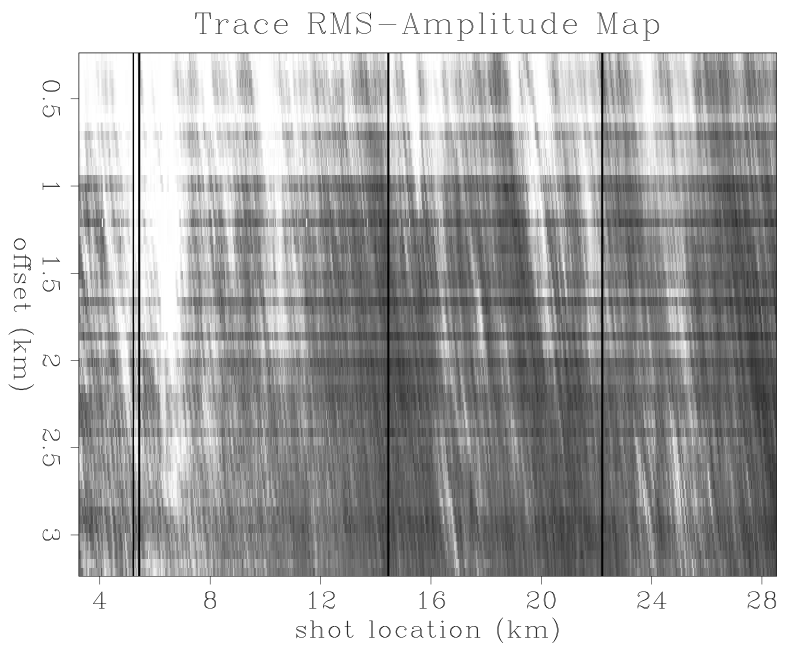

Figure 1: Trace rms-amplitude map. Horizontal stripes indicate variations in hydrophone recording sensitivity; vertical stripes indicate variations in source strength. The black vertical stripes are dead shot gathers. david1-amp1 [ER]

Amplitude model

Lumley and Berlioux present their results of source- and receiver-consistent trace amplitude balancing. Their method first removes the low-wavenumber geologic trend from source- and receiver-consistent amplitude terms by 2-D median filtering to remove noise spikes, followed by triangular smoothing of the trace rms-amplitude plane. Then the shot and receiver correction coefficients are calculated by stacking logarithmic trace amplitudes along the shot and receiver axes separately. The method is based on a simple theoretical model of trace rms amplitudes:

$$A_t(\mathbf{x}_s,\mathbf{x}_r) \;=\; A_s(\mathbf{x}_s) \,\cdot\, A_r(\mathbf{x}_r) \,\cdot\, A_e(\mathbf{x}_s,\mathbf{x}_r) \,\cdot\, A_n(\mathbf{x}_s,\mathbf{x}_r)\,. \tag{1}$$

This model is similar to that of Taner and Koehler (1981), where A_t is the trace rms amplitude response at a particular shot and receiver location $\mathbf{x}_s$ and $\mathbf{x}_r$, given as the product of a source-consistent term A_s, a receiver-consistent term A_r, and non-source-receiver-consistent terms caused by variable-reflection-strength earth geology A_e and random or coherent noise A_n. A 2-D map of A_t can be made by finding the rms amplitude of samples at each $(\mathbf{x}_s,\mathbf{x}_r)$ trace location within a specified time gate, as previously described, and shown in Figure **??**.

Regional geology trend

It is convenient to express (1) as a sum in the logarithmic domain,

$$a_t \;=\; a_s + a_r + a_e + a_n \;, \tag{2}$$

where

$$a_* \;=\; \log(A_*)\,. \tag{3}$$

If an estimate can be made of the amplitude component due to variable reflection geology strength, $A_e(\mathbf{x}_s,\mathbf{x}_r)$, then this regional geologic trend can be subtracted from (2) resulting in,

$$\hat{a}_t \;=\; a_t - a_e \;=\; a_s + a_r + a_n \;, \tag{4}$$

where we further assume $\hat{A}_t$ has been scaled to a mean value of unity. We estimate the geology contribution $A_e(\mathbf{x}_s,\mathbf{x}_r)$ by first median-filtering the trace amplitude map $A_t(\mathbf{x}_s,\mathbf{x}_r)$ to remove noise spikes, and then smooth the result with a 2-D triangular operator to get the low spatial-frequency trend. Our estimate of A_e obtained this way is shown in Figure **??**. The estimate of the trace amplitude without the bias of the geologic trend, $\hat{A}_t$, is shown in Figure **??**. This is equivalent to dividing the image of Figure **??** by the image in Figure **??**, or subtracting in the logarithmic domain. The 2-D geologic trend removal has highlighted the horizontal bands related to receiver amplitude variation.

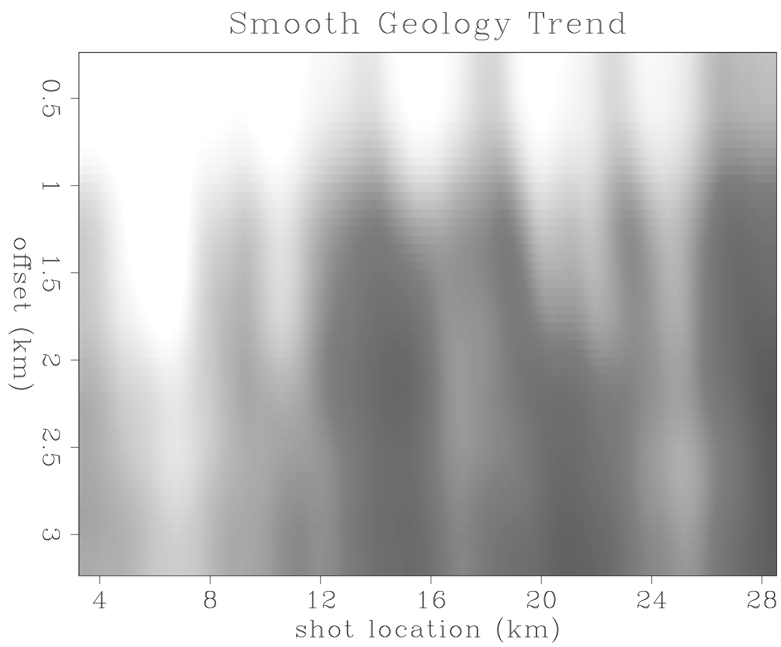

Figure 2: Low spatial-frequency regional geology amplitude trend. david1-trend [ER]

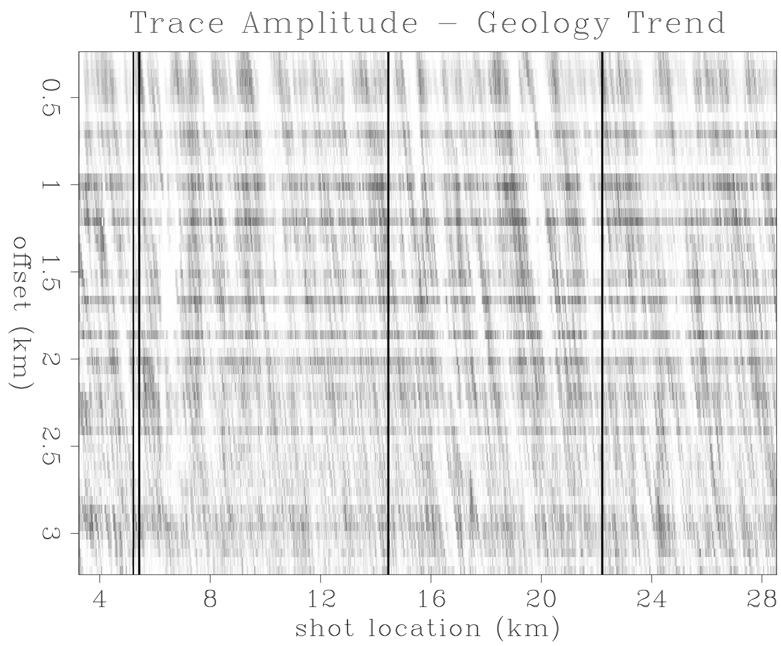

Figure 3: Unbiased trace amplitude obtained by removing the low-frequency regional geology trend. david1-amp2 [ER]

Shot and receiver coefficients

If the noise a_n is uncorrelated in both the shot and receiver axis directions, then estimates of the source and receiver amplitude balancing coefficients a_s and a_r can be obtained by directional stacking in the $\hat{a}_t$ plane. Normalized stacking along the shot axis gives an estimate of a_r,

$$a_r(\mathbf{x}_r) \approx 1/N_s \sum_{\mathbf{x}_s} \hat{a}_t(\mathbf{x}_s, \mathbf{x}_r), \tag{5}$$

if a_s and a_n are uncorrelated and zero-mean in the shot direction. Similarly, stacking along the receiver axis gives an estimate of a_s,

$$a_s(\mathbf{x}_s) \approx 1/N_r \sum_{\mathbf{x}_r} \hat{a}_t(\mathbf{x}_s, \mathbf{x}_r), \tag{6}$$

if a_r and a_n are uncorrelated and zero-mean in the receiver direction. The estimated shot and receiver coefficients are plotted in Figures **??** and **??** respectively. These are obtained by stacking Figure **??** along the receiver and shot axes respectively. The shot coefficients vary in amplitude less than 10% due to varying source strength, whereas the receiver coefficients vary up to almost 20% due to variable group cable sensitivity.

Amplitude balanced results

The final amplitude balancing coefficients $c_s(\mathbf{x}_s)$ and $c_r(\mathbf{x}_r)$ can be obtained by exponentiating and inverting a_s and a_r:

$$c_* = \exp(-a_*). \tag{7}$$

A plot of the combined source-receiver coefficients, $c_s \cdot c_r$ is shown in Figure **??**. Both vertical (source) and horizontal (receiver) stripes are clearly visible. Each seismic trace $P(\mathbf{x}_s, \mathbf{x}_r)$ can now be balanced in a source-receiver-consistent manner such that

$$\hat{P}(\mathbf{x}_s, \mathbf{x}_r) \approx c_s(\mathbf{x}_s) \cdot c_r(\mathbf{x}_r) \cdot P(\mathbf{x}_s, \mathbf{x}_r), \tag{8}$$

where $\hat{P}(\mathbf{x}_s, \mathbf{x}_r)$ is the balanced trace data. Figure **??** shows the source- and receiver-consistent balanced trace amplitude map. By direct comparison with Figure **??**, we can see that the original source and receiver variations have been largely suppressed.

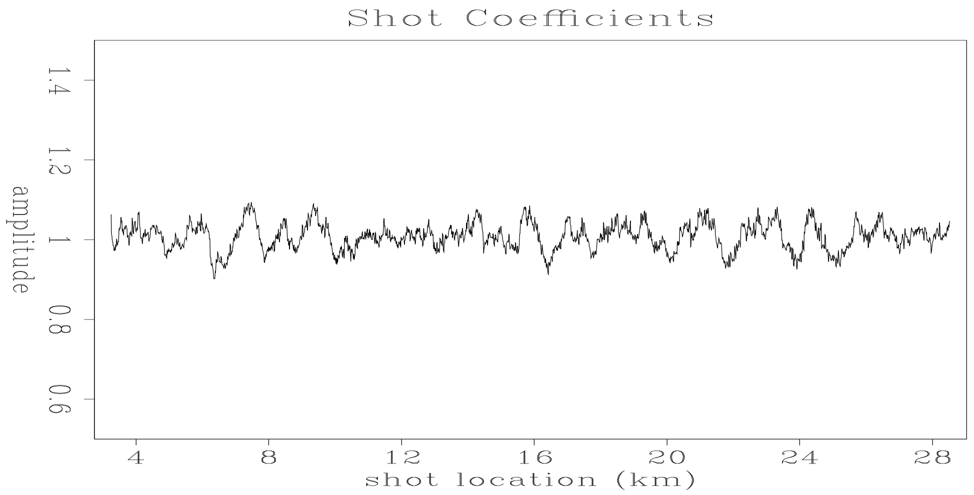

Figure 4: Shot coefficients. david1-scoeffs [ER]

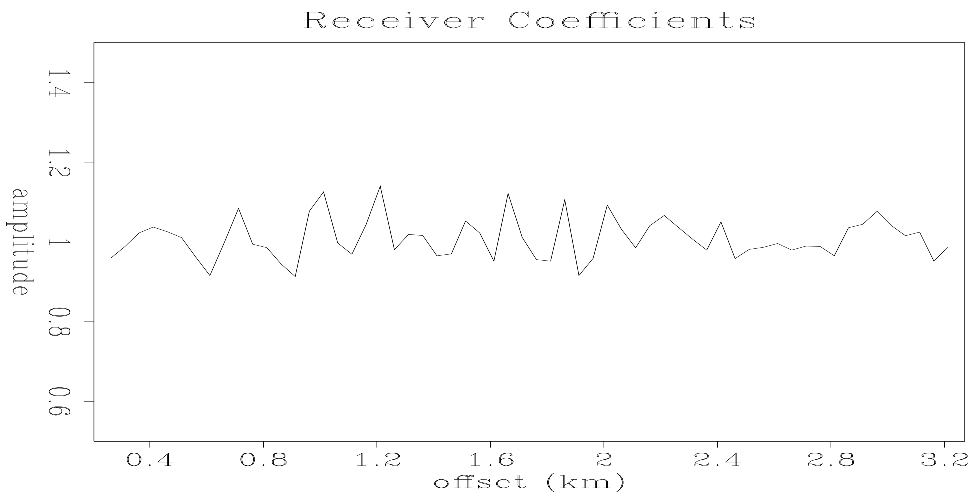

Figure 5: Receiver coefficients. david1-rcoeffs [ER]

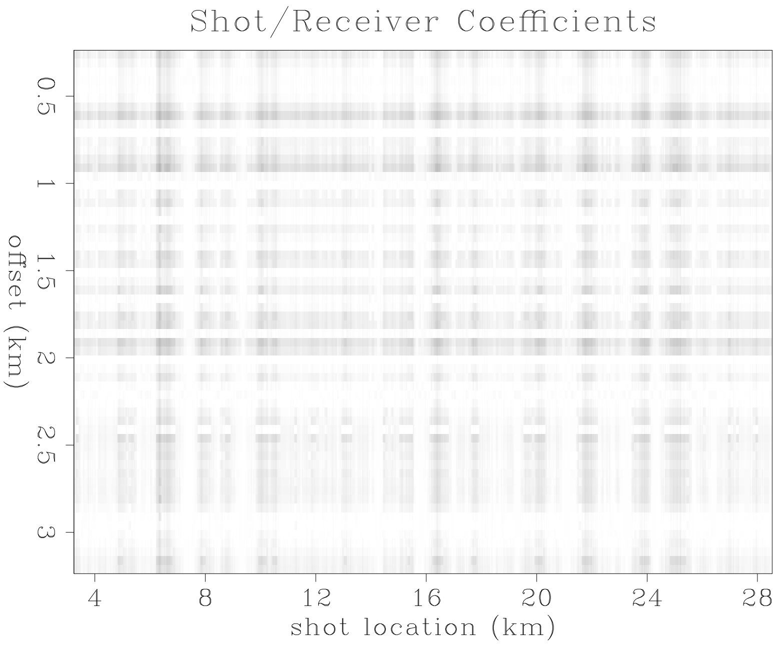

Figure 6: Source and receiver amplitude balancing coefficients. david1-acoeffs [ER]

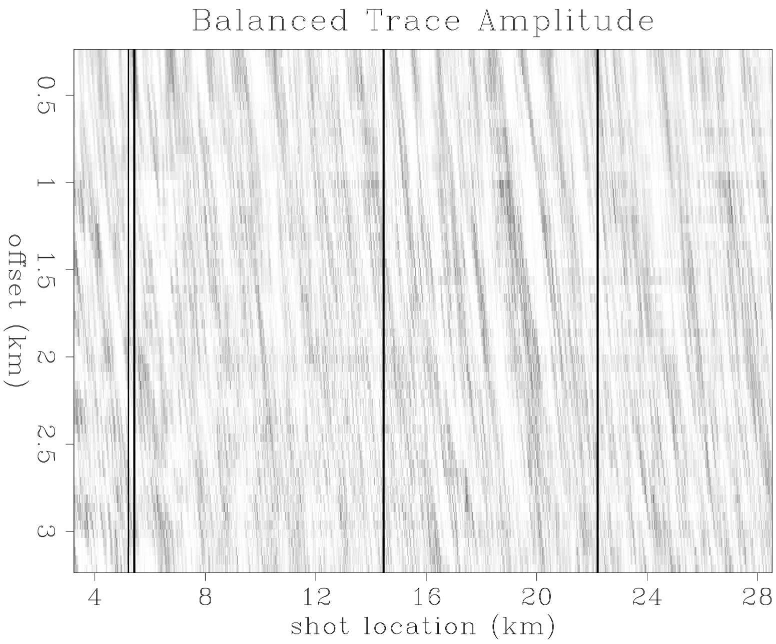

Figure 7: Balanced trace amplitude map with geologic trend removed. david1-amp3 [ER]

MULTIPLE SUPPRESSION

Multiple contamination

Water-bottom pegleg multiples distort primary reflections and contaminate the AVO character in the Mobil data. The adverse effects of multiples can be seen in the raw CMP gather and its semblance scan in Figure **??**. From drilling results, two reservoir target reflections are expected to be visible at about 2.1 and 2.6 seconds in the data, but they are almost completely masked by water-bottom pegleg multiple reflections. The companion velocity scan shows strong semblance energy associated with multiples at a wide range of traveltimes and stacking velocities, which contaminates primary stacking velocity analysis. Before accurate velocity, AVO and migration/inversion analysis can be performed, multiple reflection events need to be suppressed from the data while *simultaneously* preserving primary reflection AVO amplitudes.

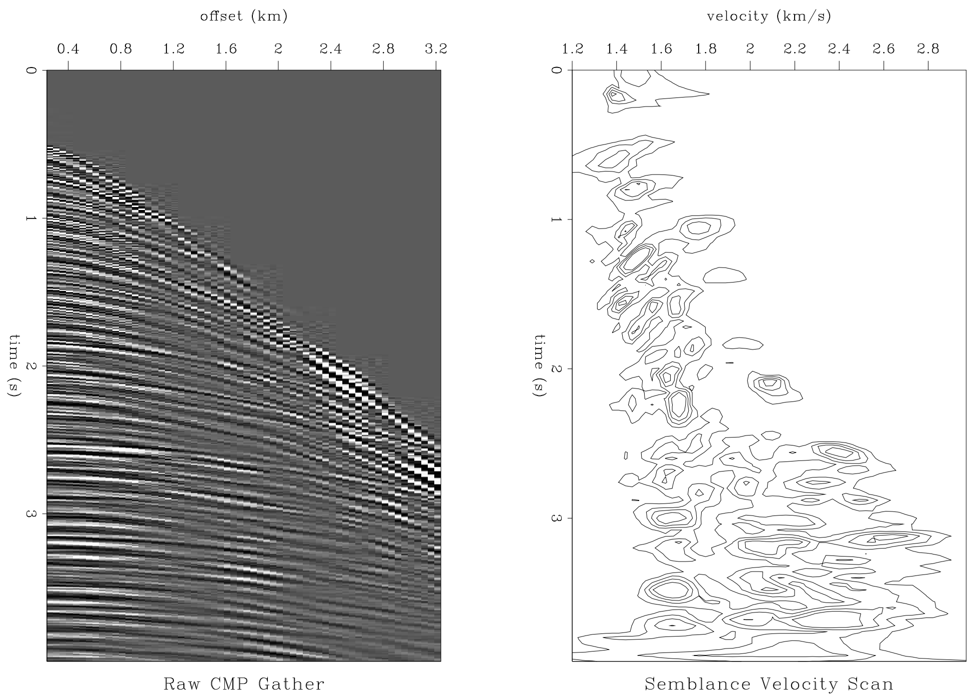

Figure 8: Mobil CMP gather and its semblance velocity scan. Reservoir target reflections are expected at 2.1 and 2.6 seconds from drilling information. david1-mocmp-semb [ER]

Multiple-suppression method

Lumley, Nichols and Rekdal (1994; 1995) present their method of amplitude-preserved multiple suppression. An iterative time-domain conjugate gradient scheme is used to invert for a velocity scan which "fits" its associated CMP gather to within a few percent misfit error, when a hyperbolic forward modeling operator is applied to that velocity scan. This ensures that most amplitude and AVO information is accurately preserved by the velocity transform pair. Next, a primary velocity trend is automatically picked in the scan by a Monte Carlo method, and a semblance mask is designed on this basis to isolate multiple energy in velocity space. The amplitude-preserved multiple-suppressed CMP gather is then obtained by modeling the isolated multiple reflections and subtracting them from the original CMP gather.

Multiple-suppression theory

The method is based upon a space-time operator which models both multiple and primary reflections as time-variant Dix hyperbolas. The hyperbolic summation/scatter operator $\mathbf{H}$ maps points in the velocity model space $\mathbf{m}(\tau, v)$ to a CMP gather in the seismic data space $\mathbf{d}(t, h)$:

$$\mathbf{d} = \mathbf{H}\mathbf{m} , \tag{9}$$

where h is source-receiver offset, t is two-way traveltime, v is Dix rms velocity, and τ is two-way vertical traveltime (pseudodepth). Since the operator $\mathbf{H}$ resides in the space-time domain, it has the advantage of being able to accurately avoid frequency-domain artifacts arising from data mute zones and dead traces. Furthermore, the hyperbolic operator allows non-stationary use of offset, time and cosine operator weighting, as well as rho-filter spectral shaping. The time-variant nature of the hyperbolic operator allows for optimal separation of primary and multiple velocity energy compared to slant-stack (**?**), parabolic (Hampson, 1986), or time-shifted hyperbolic methods, Foster and Mosher (1992). Optimal velocity separation is critical for all multiple suppression techniques based on moveout velocity difference, in both a kinematic and dynamic sense. The method is not as theoretically accurate as wave-equation derived scattering (Carvalho et al., 1991) or surface-consistent methods (Verschuur et al., 1992), but is potentially orders of magnitude faster and more stable in practical applications. This is because wave-equation methods require computing several cascaded terms of the wavefield continuation to stabilize the series expansion, need accurate estimates of the source wavefield, and require estimates of unrecorded near and far offset data to predict late offset-dependent multiple arrivals. The least-squares estimate of $\mathbf{m}$ from (9) requires minimizing the L_2 norm of the residual error,

$$||\mathbf{r}||^2 = ||\mathbf{d} - \mathbf{H}\mathbf{m}||^2 , \tag{10}$$

with respect to $\mathbf{m}$. The method of conjugate gradients (**?**) provides an iterative L_2 approximation $\hat{\mathbf{m}}$ for the exact solution $\mathbf{m}$. The CG method iterates until a velocity scan $\hat{\mathbf{m}}$ is found which fits the data upon forward modeling, to within some specified error tolerance. At this point of "practical convergence", the L_2 velocity scan can be forward-modeled with the scattering operator $\mathbf{H}$ and will accurately match the input data. Hence, an amplitude-preserving velocity transform pair has been found. Since the time-variant hyperbolic operator is optimal for separating multiple and primary energy in velocity space, multiple reflection energy may be isolated and accurately modeled from the velocity scan $\hat{\mathbf{m}}$ without seriously distorting primary energy. Multiple reflections modeled this way can then be subtracted from the input CMP gather, resulting in an amplitude-preserved multiple-suppression technique.

Multiple-suppression results

To examine the effectiveness of the multiple-suppression technique, we first tested the method on full-wave synthetic data. Once we were satisfied we had passed this test, we performed multiple suppression to the entire Mobil line. The method is fully automatic in the sense that it requires no manual interactive procedures once the run parameters are optimized (e.g., no interactive design of velocity space masks), and takes about 1 CPU minute per CMP gather on an HP 735 workstation.

Synthetic data

Figure **??** shows full waveform elastic synthetic seismograms generated at the Well A location using blocked well-log values and a 1-D Haskell-Thompson matrix propagator modeling algorithm (Aki and Richards, 1980). The left panel show data modeled without free-surface multiples, but including interbed multiples and both primary and shear-converted P-wave reflections. The right panel is the same, except it includes the free-surface multiple reflections. Figure **??** shows a comparison of the multiple suppression on the full waveform synthetic data. The left panel shows the original input data including free-surface multiples, the center panel is our amplitude-preserved multiple-suppression, and the right panel is the subtracted estimate of the multiple reflections. Kinematically, the multiple-suppression has done a good job at removing multiple reflection events. However, the method also seems to be very good dynamically in the sense that there is no obvious amplitude distortion of recovered primary events from near to far offset. Furthermore, whereas most primary events are fairly constant in amplitude, the two reservoir reflections at 2.2 and 2.6 seconds have retained the correct (and opposite trend) AVO behavior. Figure **??** shows a tough test of the method that is not available in field data situations. The left panel is the full waveform data modeled *without free-surface multiples*, the center panel is the multiple-suppressed data of Figure **??**, and the right panel is the unweighted subtraction of the two to make the residual data, all plotted at the same scale. Any amplitude error in the multiple-suppressed data in the offset or time direction will cause reflection events to appear in the residual data. However, the residual data is comprised mostly of incoherent noise. There are faint traces of residual multiple reflection events at the very near offsets, and some residual shear-converted energy that occurs at moveout velocities lower than what was modeled in the L_2 velocity scans. This is our best evidence that the method appears to perform very well at removing multiple reflections while simultaneously preserving AVO amplitudes.

Field data

Figure **??** shows an application of our method to a single CMP gather from the Mobil data set. The left panel shows the input data in which multiple reflections mask the primary target events at 2.1 and 2.6 seconds. The center panel shows our multiple-suppressed estimate, and the right panel shows the subtracted multiples. The three prominent events at 1.8, 2.1 and 2.6 seconds have been cleaned up in the multiple-suppressed version. Also, the top reservoir reflection at

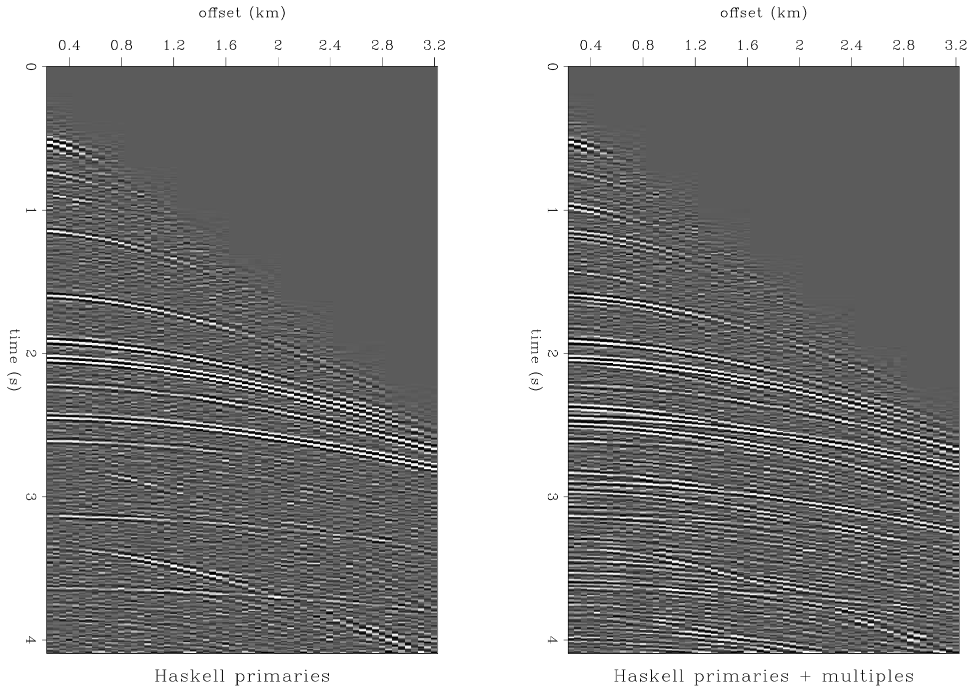

Figure 9: Haskell synthetic CMP gathers. "Primaries" gather (left) is modeled without free-surface multiples, but includes interbeds and shear conversions. The gather on the right includes the extra free-surface multiples. The reservoir reflections at 2.2 and 2.6 seconds have the correct opposite AVO trends. david1-hpm-cmp [ER]

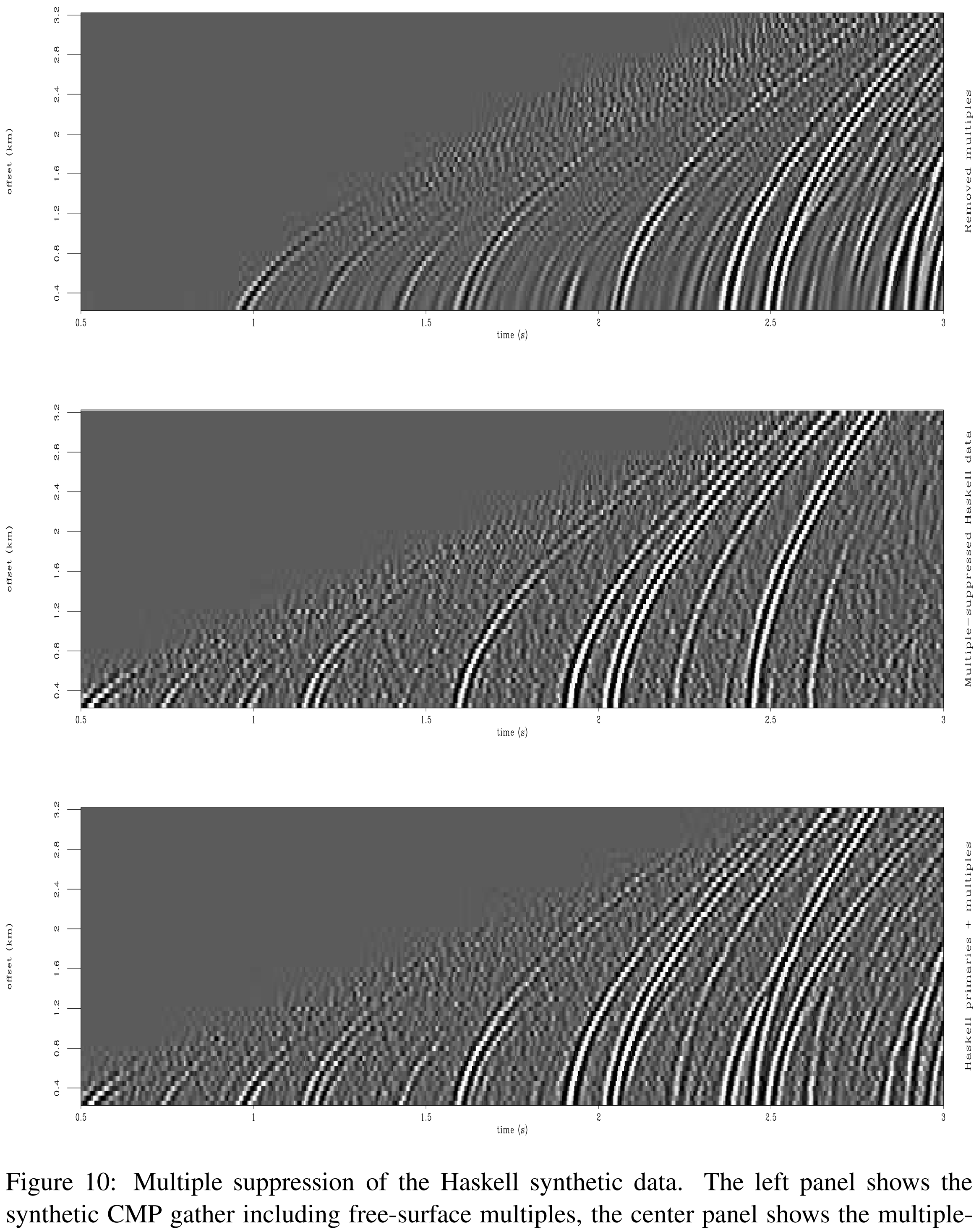

Figure 10: Multiple suppression of the Haskell synthetic data. The left panel shows the synthetic CMP gather including free-surface multiples, the center panel shows the multiple-suppressed data, and the right panel shows the removed multiples. The target AVO trends at 2.2 and 2.6 seconds have been correctly preserved. david1-hask1 [ER,M]

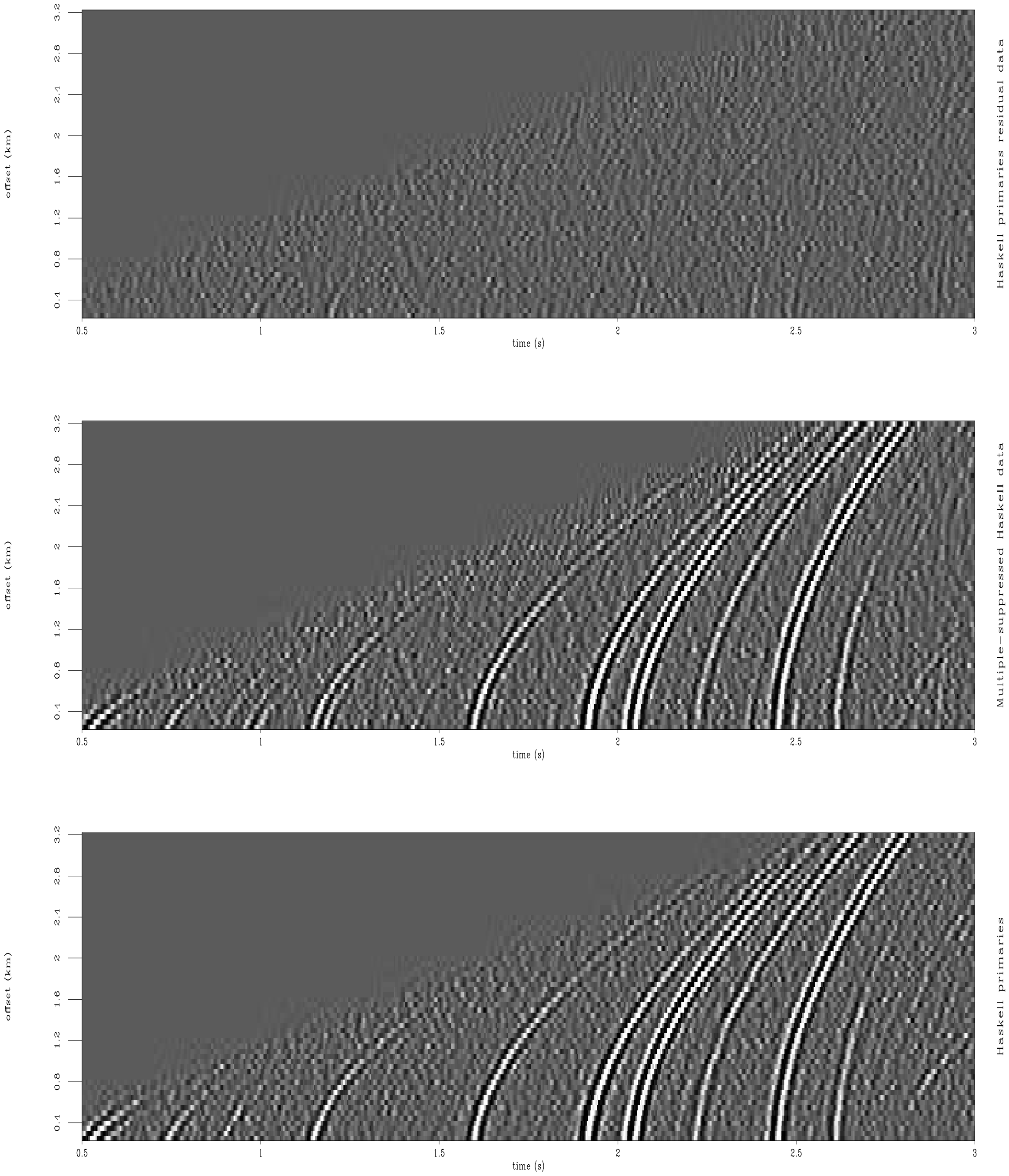

Figure 11: Multiple suppression of Haskell synthetic data. The left panel is the original CMP gather modeled without free-surface multiples, the center panel is the multiple-suppressed data, and the right panel shows the residual (difference) between the two, all at the same scale. Since the multiple-suppressed data accurately matches the ideal multiple-free synthetics, the residual data contains mostly incoherent noise. $\boxed{\text{david1-hask2}}$ [ER,M]

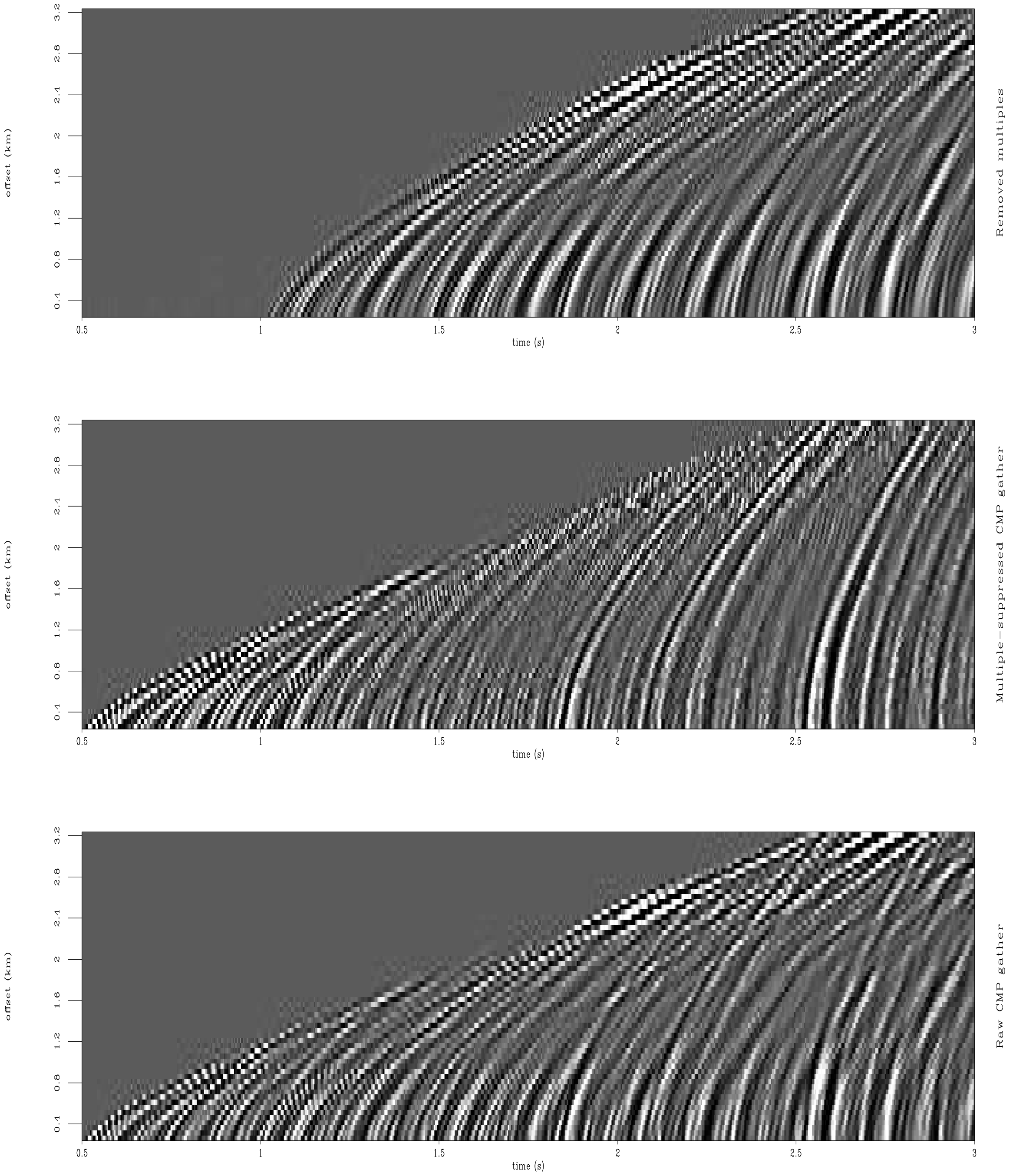

Figure 12: Multiple suppression of the Mobil CMP gather. The left panel shows a raw input CMP gather, the center panel shows the multiple-suppressed data, and the right panel shows the removed multiples. The AVO trends on the target reflections at 2.1 and 2.6 seconds seem reasonable. Also, the radial birefringence pattern characteristic of water-column pegleg multiples is visible in the estimated multiples, but not the primaries. $\boxed{\text{david1-mobil}}$ [ER,M]

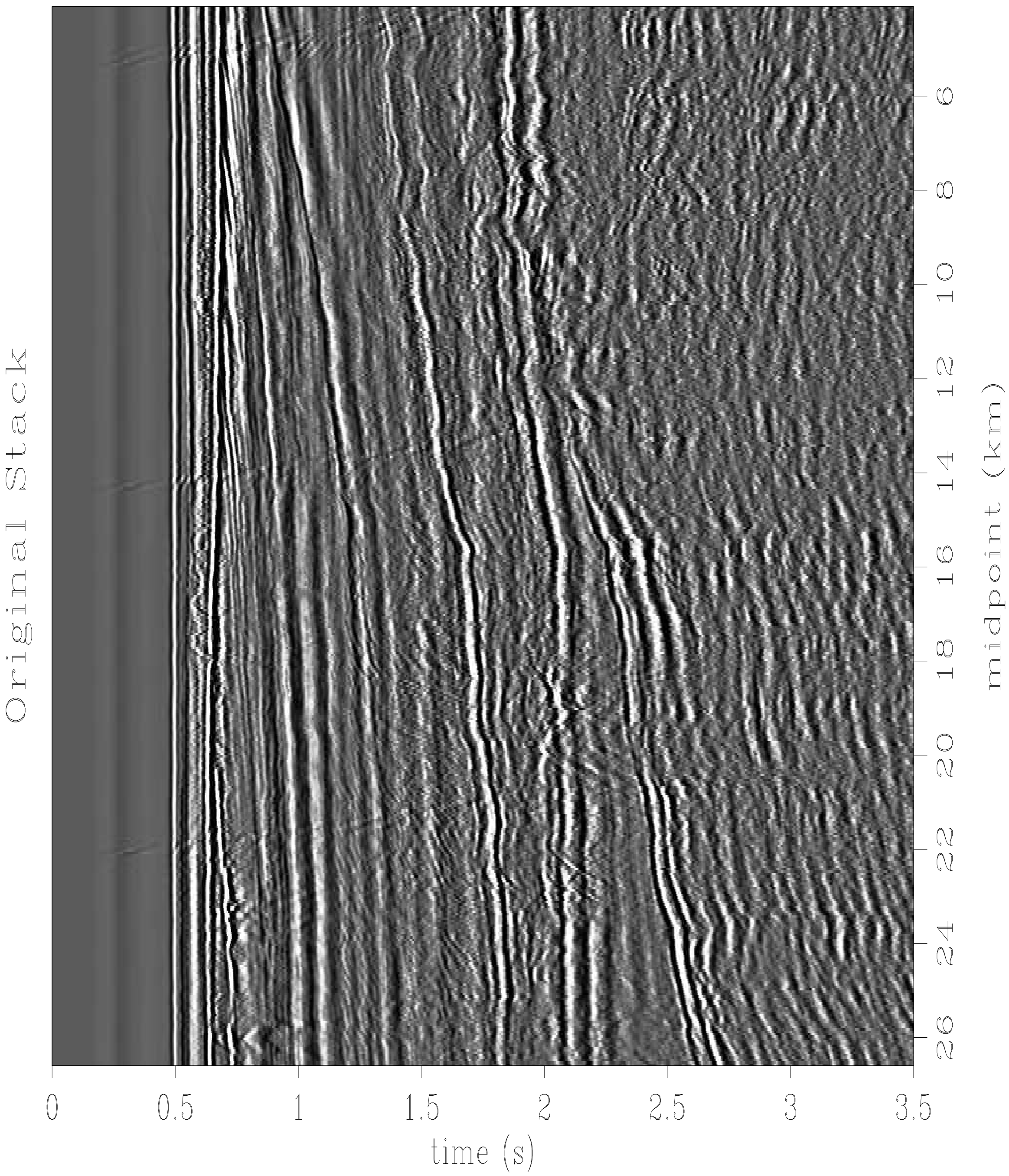

Figure 13: Stacked section before multiple suppression. Deep reflections below the unconformity are masked. david1-stack1 [ER,M]

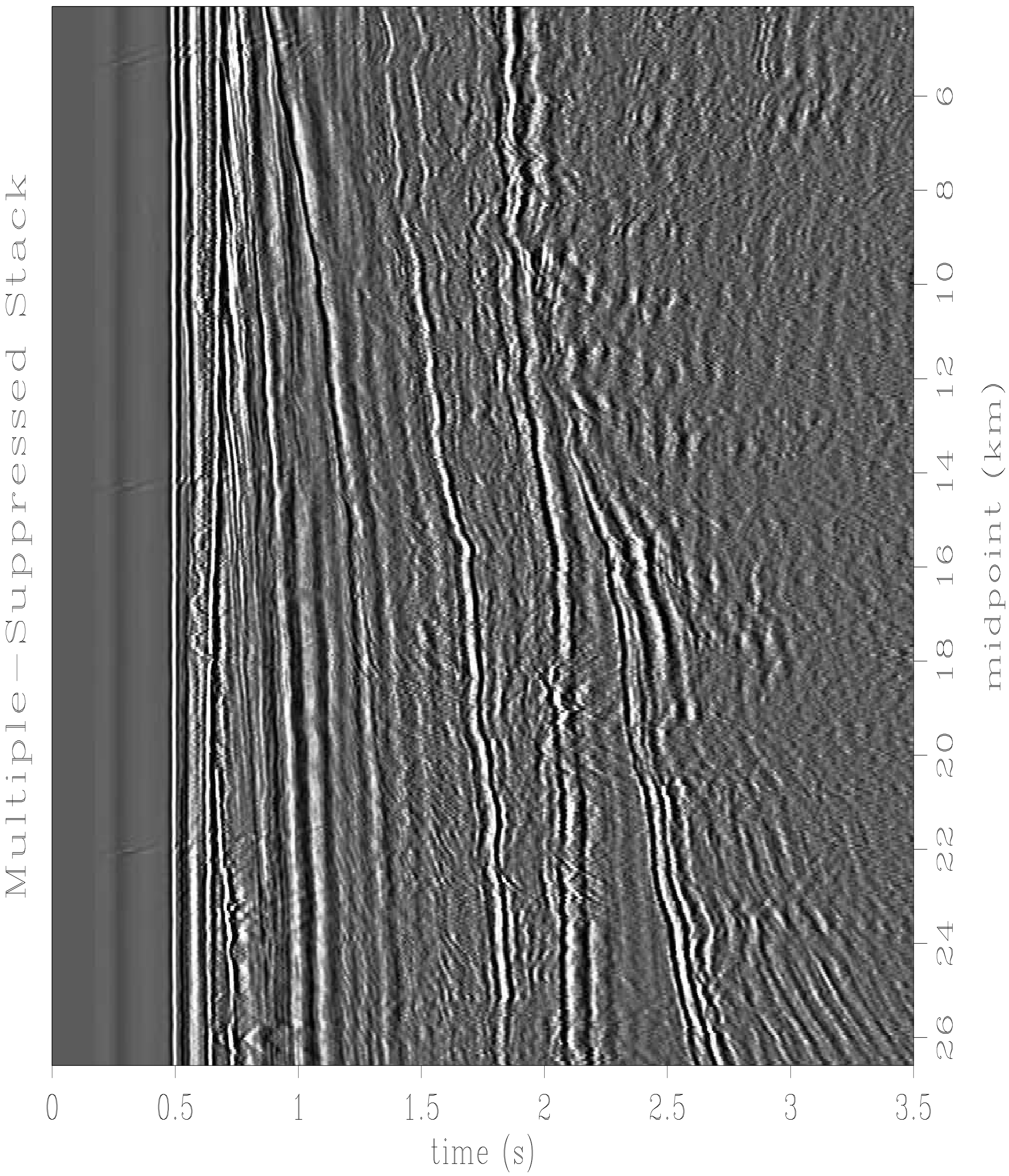

Figure 14: Stacked section after multiple-suppression. Deep reflections associated with horst-graben structure underneath the unconformity have been recovered. $\boxed{\text{david1-stack2}}$ [ER,M]

2.1 seconds has the expected amplitude-increasing-with-offset AVO behavior, and the lower target at 2.6 seconds has the expected opposite amplitude-decreasing-with-offset AVO trend, as predicted by full waveform modeling from the well logs. Another point of interest is that the raw input gather has a radial birefringence pattern that is typical of water-column multiples: amplitudes are brighter at the near and far offsets, yet weak in the middle offsets. The x–t radial periodicity of this effect is controlled by the water depth and the source bandwidth. The estimated multiple reflections in the right panel exhibit this radial birefringence pattern, but that the multiple-suppressed primaries in the center panel do not. For comparative purposes, Figures **??** and **??** show stacked sections of the Mobil data made before and after multiple-suppression respectively. As is often the case, stacking is such a powerful noise-suppression method that it tends to attenuate multiples sufficiently well in stacked sections. However, the multiple-suppression has definitely cleaned up deeper parts of the section, especially in the region of horst-graben faulting at 2.5–3.5 seconds and midpoints 20–26 km. A stacked section comparison is mainly kinematic and gives little indication of dynamic AVO amplitude preservation in the multiple suppression, as will be demonstrated in the subsequent AVO analysis and migration/inversion sections. In summary, our multiple-suppressed gathers clearly show recovered primary reflection events with reasonable AVO behavior, and the estimated multiple reflections show radial birefringence patterns characteristic of water-column pegleg multiples. The stacked sections show that the multiple suppression has cleaned up deeper parts of the structure associated with horst-graben faulting. This combined evidence suggests that our multiple-suppression method works well on both synthetic and field data.

UNMIGRATED AVO ANALYSIS

Lumley and Ecker present their results of conventional unmigrated AVO analysis applied to the Mobil data. AVO gathers were examined before and after multiple suppression. Hydrocarbon indicator (HCI) sections were computed using near and far offset AVO amplitudes to try and highlight the top reservoir reflection in both cases. The multiple-suppressed AVO analysis gives a cleaner HCI section, and indicates a possible undrilled reservoir in the center graben block.

Unmigrated AVO gathers

Figure **??** shows amplitude-corrected unmigrated AVO gathers near the Well A location, and Figure **??** shows the same near the Well B location, before and after multiple suppression. Two iterations of stacking velocity analysis were performed: one before and one after multiple suppression. All multiple-suppressed gathers are NMO-corrected with the better velocities obtained in the second iteration, whereas original gathers with multiples are NMO-corrected with the inferior first velocity analysis estimates. All gathers were amplitude-corrected for the effects of geometric spreading and source-receiver directivity. The left panel of Figures **??** and **??** show the unmigrated AVO gathers before multiple suppression. The right panels show the same after multiple-suppression. The source-receiver directivity correction has unreasonably gained up far offset multiple reflection amplitudes. That is because the multiples are propagating more vertically than the primaries at the far offsets, and so get overcompensated for wide-angle source-receiver directivity and geometric spreading. The two figures show that the multiple-suppressed gathers show cleaner primary reflection events, reasonable AVO amplitudes, and better moveout velocity correction; all of which should enhance AVO analysis.

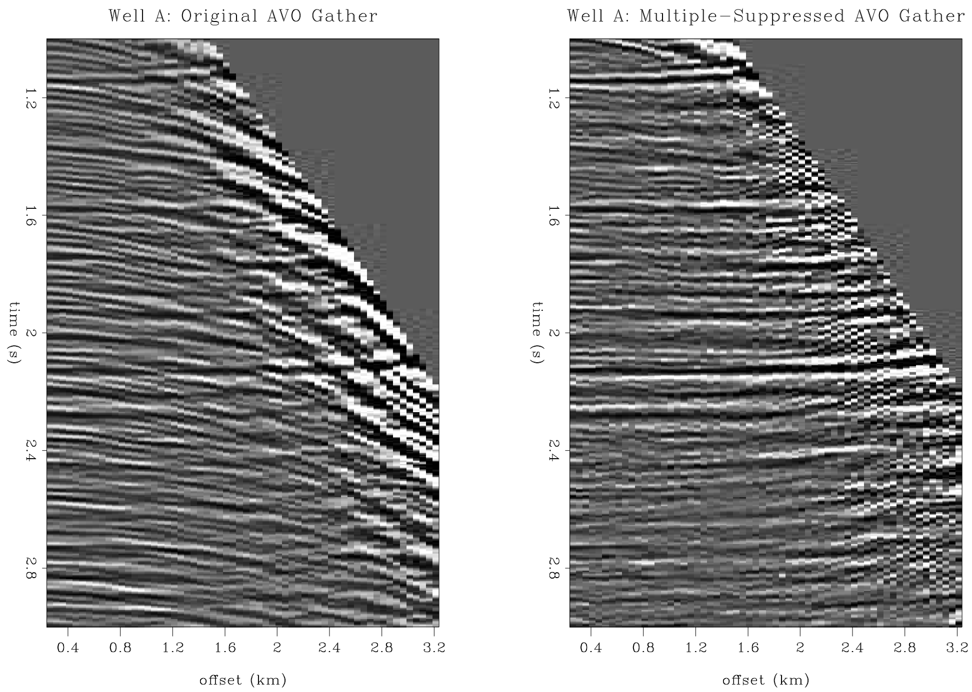

Figure 15: Unmigrated AVO gathers near Well A: before (left) and after multiple suppression (right). Multiples have been overcompensated by the source-receiver directivity correction, but the gather exhibits a clean and reasonable AVO trend after multiple suppression. david1-avo12A [ER]

Unmigrated HCI sections

HCI sections were computed using all full-fold CMP gathers along the line. Estimates of conventional (A, B) and relative-impedance-contrast parameter sections were obtained from the unmigrated AVO gathers. These showed reasonable-looking AVO structure, but did not show clean composite multi-parameter hydrocarbon indicators at the known top reservoir location. Instead, a better HCI section was obtained as follows. The amplitude-corrected gathers were partially stacked into two reflection-angle ranges: 0–15 degrees, and all angles beyond. Call these two parameter sections "near" N and "far" F. A reasonable HCI section was then obtained using the composite indicator

$$\mathrm{HCI} = N(N - F) \; . \tag{11}$$

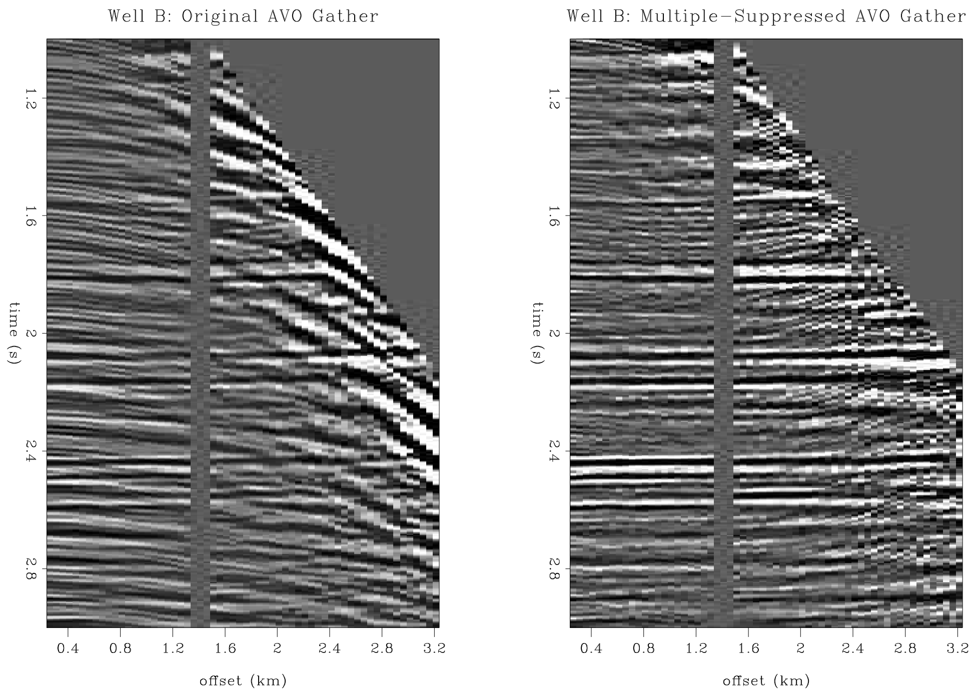

Figure 16: Unmigrated AVO gathers near Well B: before (left) and after multiple suppression (right). Multiples have been overcompensated by the source-receiver directivity correction, but the gather exhibits a clean and reasonable AVO trend after multiple suppression. $\boxed{\text{david1-avo12B}}$ [ER]

This N, F technique does not contain as much AVO information as A, B or impedance-contrast sections, but has a higher S/N ratio. Amoco has given some presentations using a similar technique in recent off-the-record workshops. Our indicator is appropriate for the top reservoir in which amplitude increases with offset. We did not attempt to refine a separate indicator which would highlight the more subtle amplitude-decreasing-with-offset AVO anomaly at the deeper reservoir target. Figure **??** shows the HCI section computed as described above for the non-multiple-suppressed data. White (red) indicates an HCI anomaly of classic amplitude increasing with offset, which is appropriate for the top reservoir. The HCI section is extremely noisy. The top reservoir event shows up as anomalous along most of the line, but unfortunately most shallower events give false anomalies too. This HCI section would be practically useless to an interpreter trying to high-grade a drilling location. Figure **??** shows the same HCI section except computed using the multiple-suppressed data. The section has been cleaned up considerably compared to Figure **??**. The shallow event at 1.6–2.0 seconds is still noisy, but the HCI anomaly at the 2.1 second reservoir reflection is clearly stronger in S/N ratio. A strong anomaly is highlighted for the first time at 2.5 seconds and 15–18 km midpoint distance. This anomaly occurs in a central graben block along the line, and as shown in the next section, its strength increases in the updip direction, and is truncated by the updip horst-graben normal fault. This HCI section would definitely be of more value to an interpreter in correlating existing well information to an AVO HCI section, and in suggesting potential new drilling locations.

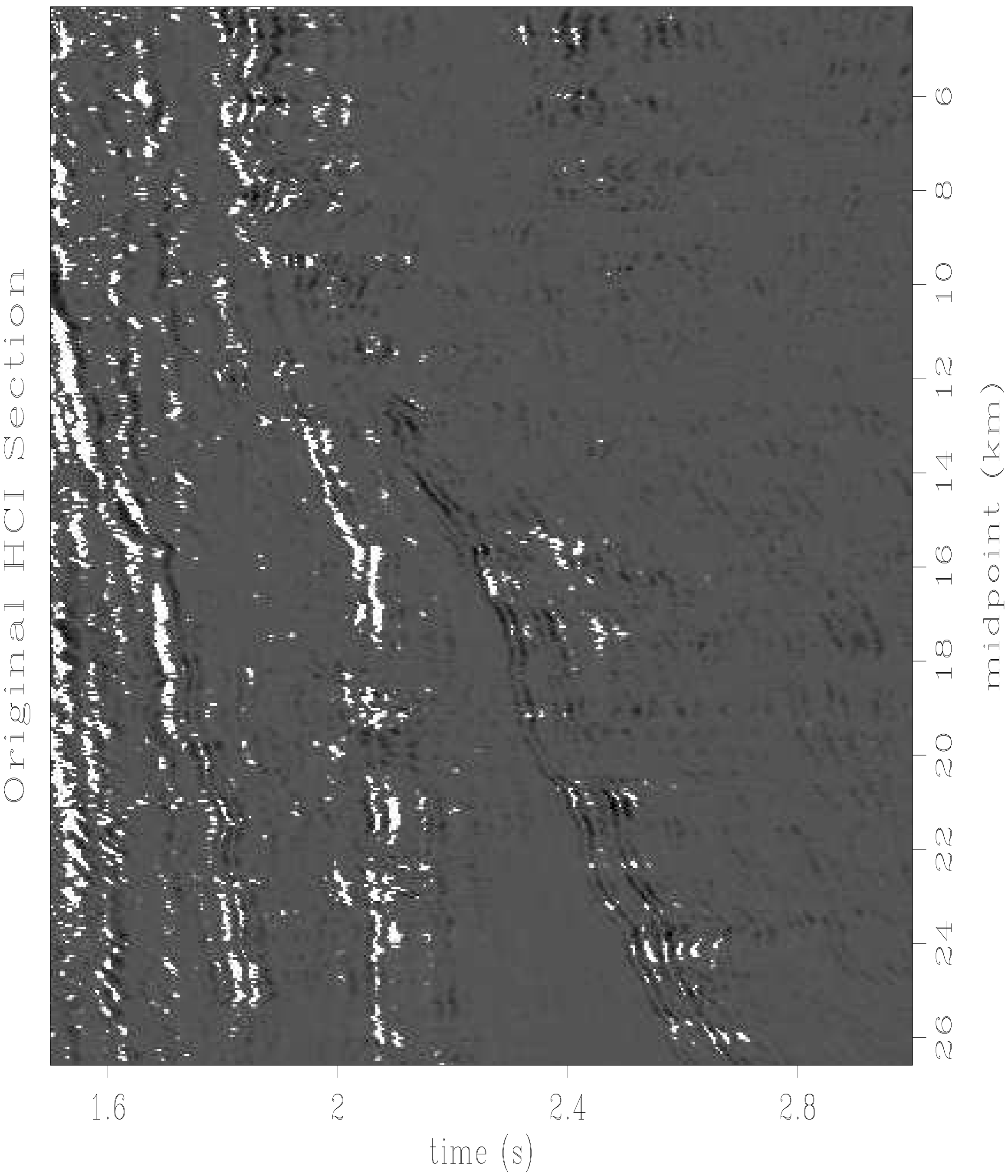

Figure 17: HCI section from unmigrated AVO analysis before multiple suppression. White (red) represents a classic AVO anomaly of amplitude increasing with offset. The section is so noisy that it is practically useless. $\boxed{\text{david1-hci1}}$ [ER,M]

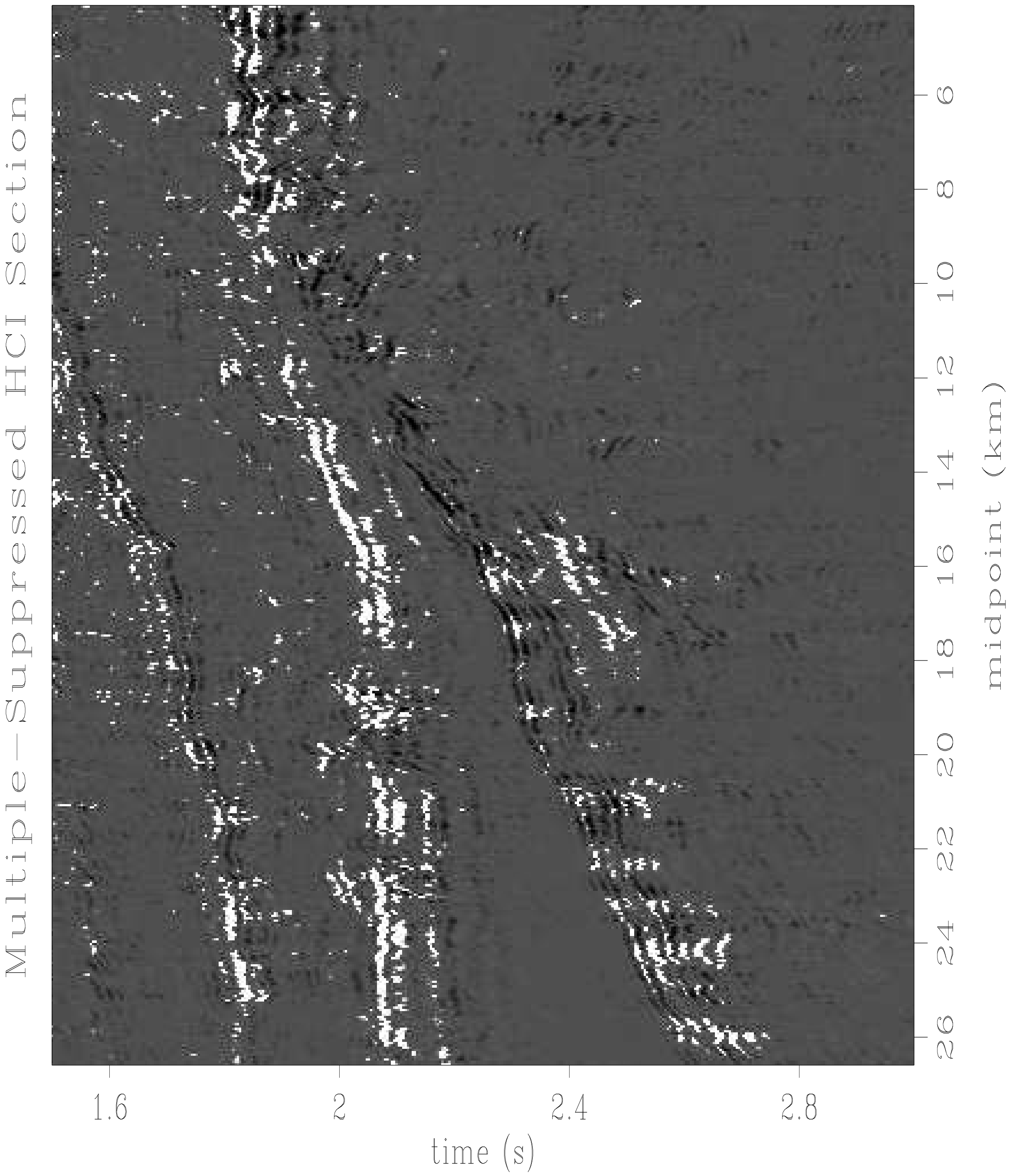

Figure 18: HCI section from unmigrated AVO analysis after multiple suppression. White (red) represents a classic AVO anomaly of amplitude increasing with offset. This section is much cleaner, and shows a strong AVO anomaly associated with the known reservoir at 2.1 seconds. Note the new anomaly in the graben at 2.5 seconds and 15–18 km. $\boxed{\text{david1-hci2}}$ [ER,M]

PRESTACK MIGRATION/INVERSION

Migration/inversion method

Lumley presents his Kirchhoff prestack migration/inversion method applied to the multiple-suppressed Mobil data. This method is based on previous amplitude-preserved prestack depth migration and impedance inversion work, Lumley (1989; 1993a; 1993b), and is related to works by Bleistein (1987), Beydoun and Mendes (**?**), and recently Schleicher et al. (**?**). The method can operate in either the prestack time or depth migration domains, and compensates internally for geometric spreading and source-receiver directivity in a wave-equation consistent manner. Estimates of both reflection angle and reflection amplitude are provided, and are combined as a function of offset and (pseudo)depth to give the total angle-dependent reflectivity estimate. Elastic and AVO parameter estimates can be obtained as a second step given the migration/inversion angle-dependent reflectivity estimates as input. For the Mobil data application, we performed amplitude-preserved prestack time migrations of constant-offset sections. Time migration was favored over depth migration because of its speed and robustness in this laterally-smooth velocity field. Sixty input offset sections were prestack-migrated into ten output offset sections, in a pseudodepth window of 1–3 seconds vertical traveltime. The migration takes about the same CPU run time as a standard Kirchhoff prestack time migration, but uses three times the memory to store the multiple images necessary to calculate the amplitude-preserved reflectivity and reflection-angle estimates.

Migration/inversion results

Figure **??** shows an example of a prestack migration/inversion reflectivity (left) and reflection angle iso-x gather (right) located at 15.768 km midpoint distance, in the vicinity of the central graben. An enlarged view of the reflection AVO response is shown in Figure **??**. The top reservoir reflection at 2.05 seconds clearly exhibits a classic AVO response of amplitude increasing with offset, as predicted by the full waveform synthetic and the available well-log data. The reflection at the major unconformity at 2.25 seconds also has increasing AVO with offset, which may indicate hydrocarbon content, or perhaps a large shear impedance decrease due to overpressure across the unconformable boundary. The large reflection at 2.45 seconds has a large increase in amplitude with offset corresponding to the updip segment along the down-thrown graben, very near to the updip horst-graben fault truncation as shown in Figures **??** and **??**. This classic AVO response suggests that perhaps gas-charged hydrocarbons have accumulated updip in this graben structure. Just below this “gas” reflection, there is a reflection at 2.50 seconds, best viewed in Figure **??**, which seems to exhibit a polarity reversal. It starts off positive at near offsets, has a zero crossing at about 1.3 km offset, and becomes strongly negative at far offsets. This AVO behavior is consistent with an oil-water contact, and may represent the base of the oil/gas zone at this location. We have labeled this location as “Well D” for Mobil interpreters to consider as a future drilling prospect.

Using the migrated AVO and angle gathers from the prestack migration/inversion, an HCI section was computed in an analogous manner to the description in the previous section. Fig-

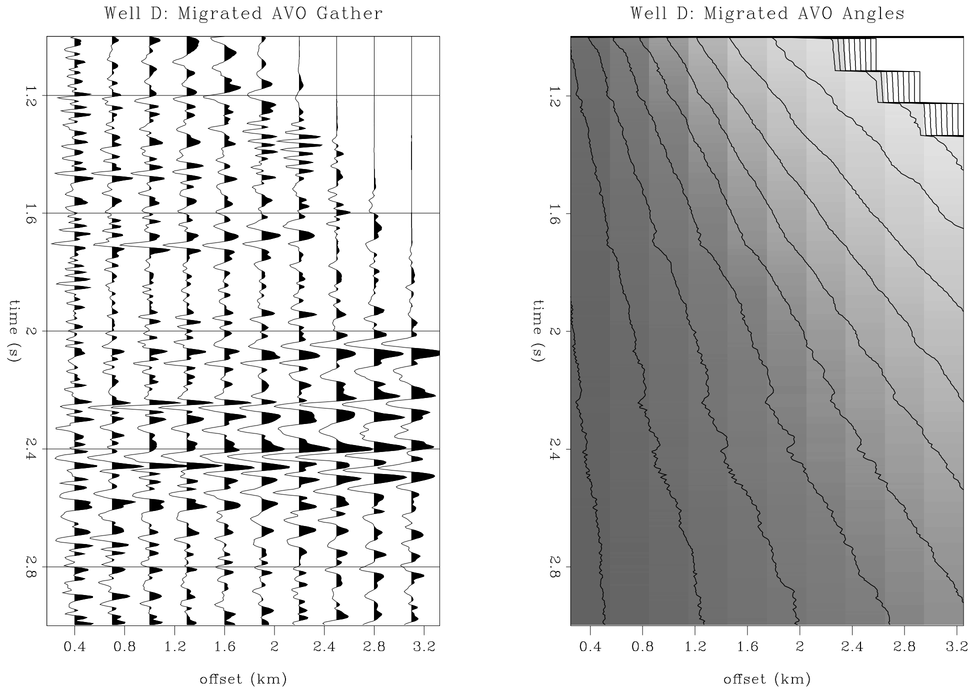

Figure 19: Migration/inversion reflectivity (left) and reflection angle gathers (right), located near the central graben. The angle contours start at 5 degrees at the near offset and increase in 5 degree increments. There is about 35 degrees of reflection illumination angle at 2.0 seconds pseudodepth. david1-avo3 [ER]

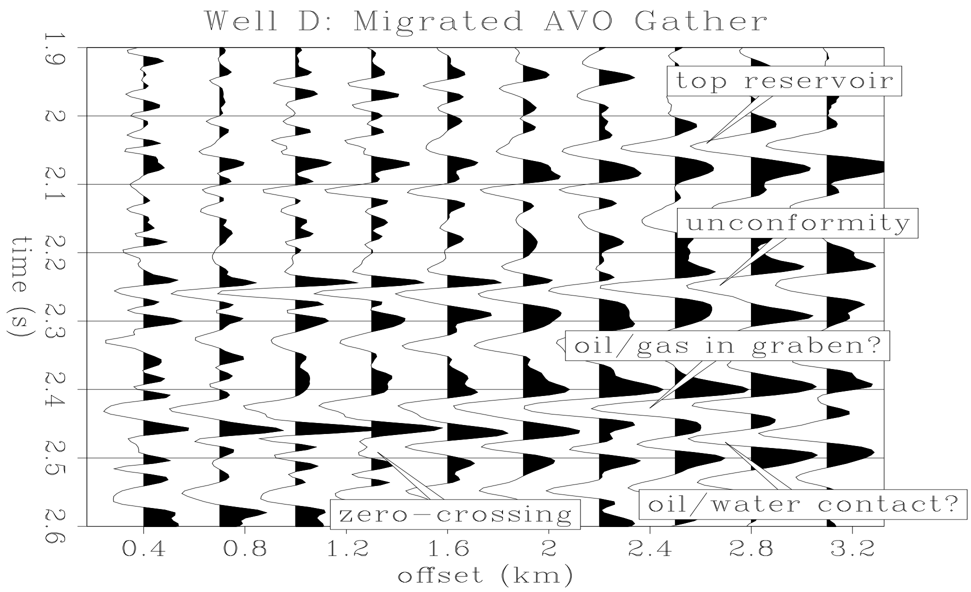

Figure 20: An enlarged view of the migration/inversion reflectivity AVO response. The proposed oil/gas reflection in the graben has a strong classic amplitude increase with offset. A possible oil/water contact reflection has a characteristic polarity reversal with offset. david1-avo3b-ann [ER]

ure **??** shows the migration/inversion HCI result. The HCI section is much cleaner than the unmigrated analysis of Figure **??**. The shallow event at 1.6–2.0 seconds is now nearly completely devoid of a false hydrocarbon anomaly, yet the top reservoir event at 2.1 seconds still correctly shows a strong anomaly along the line. The deep AVO anomaly at 2.5 seconds in the center of the line is also much stronger than the unmigrated AVO analysis shows, and the truncation at the updip horst-graben fault is now clearly in focus. Figure **??** shows a stack of all the amplitude-preserved prestack-migrated reflectivity gathers. Note the near-vertical faulting at the right side of the section under the unconformity. The down-thrown graben block in the center at 2.5 seconds from 15–20 km is now clearly visible, and the amplitude of the dominant negative reflection seems to increase in brightness in the updip direction. Both the amplitude-preserved migrated section and the migration/inversion HCI section are consistent with gas accumulated updip, trapped against the updip horst-graben normal fault. In this example, the combination of amplitude-preserved multiple-suppression and prestack migration/inversion seem to provide much better information needed to high-grade drilling locations than unmigrated AVO analysis or non-amplitude-preserved multiple attenuation.

CONCLUSION

We have focused on amplitude-preserved processing and analysis of the Mobil AVO data. We have shown that source-receiver consistent amplitude variations are as large as 10% and 20% respectively, and have demonstrated a quick and robust method for performing the required amplitude balancing corrections. Multiple reflections seriously contaminate primary AVO response in the Mobil data in CMP gather and HCI section comparisons. We developed a new method for suppressing undesirable multiple reflections while preserving AVO information along primary reflection events. The method is derived from least-squares conjugate-gradient inverse theory applied to time-variant Dix hyperbolic operators, and was shown to be effective on full waveform synthetics and the Mobil field data. Finally, we showed that prestack migration/inversion analysis is superior to unmigrated AVO analysis of the Mobil data. Our results correlate with a known reservoir reflection from well-log data, and we find what appears to be an as-yet undrilled hydrocarbon reservoir in a large central graben block underlaying the major structural unconformity.

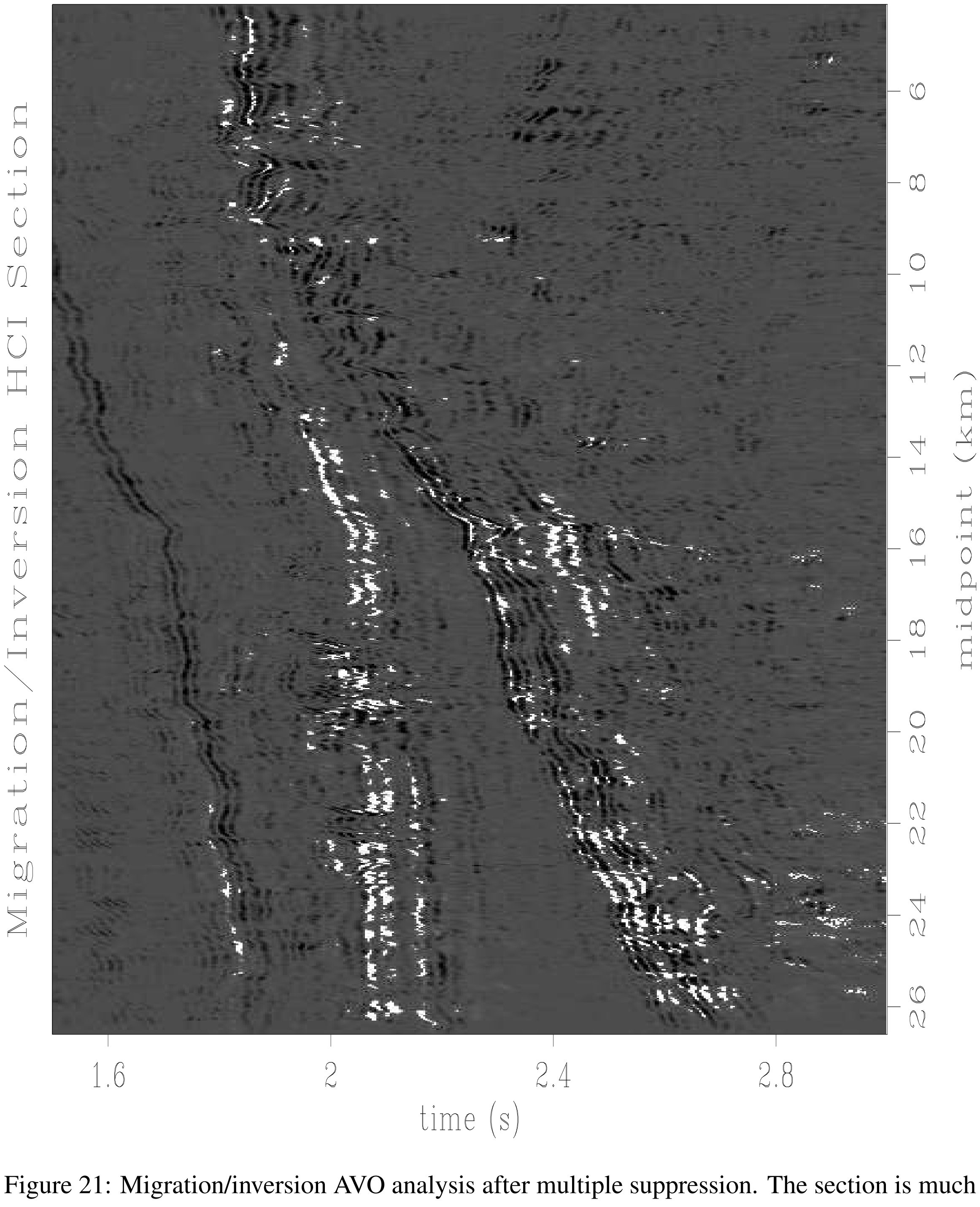

Figure 21: Migration/inversion AVO analysis after multiple suppression. The section is much cleaner than either unmigrated AVO analysis sections, and that the top reservoir at 2.1 seconds is strongly anomalous as expected from well log data. The new HCI anomaly at 2.5 seconds in the central graben is clearly truncated updip by the horst-graben fault. david1-hci3 [ER,M]

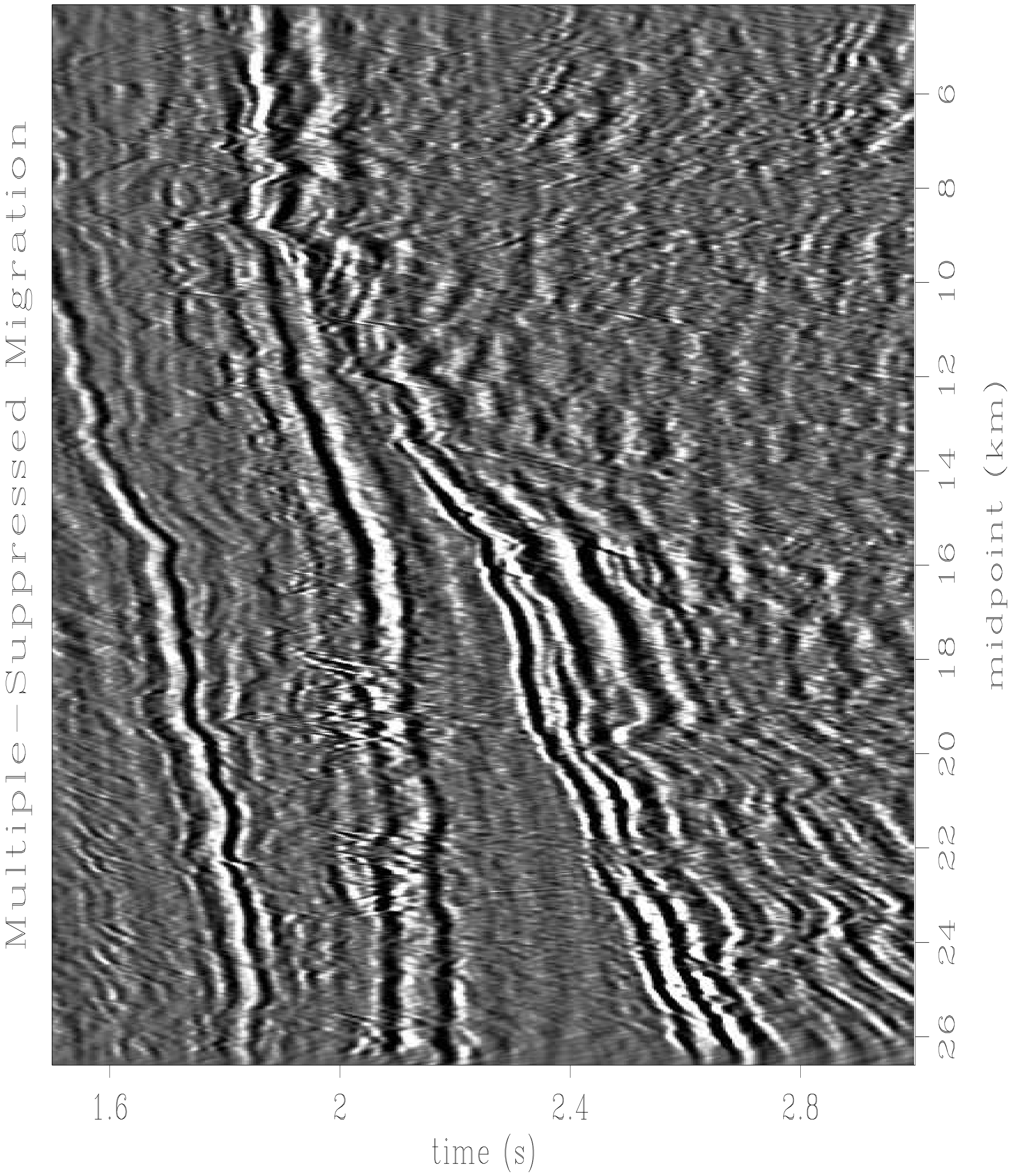

Figure 22: Amplitude-preserved prestack migration. Note the near-vertical faulting to the right of the section under the unconformity. Also note that the negative reflection at 2.5 seconds in the central graben becomes increasingly bright updip, and is truncated against the horst-graben fault. This is consistent with gas-charged hydrocarbons accumulating updip, and represents a potentially new drill-site location. david1-mig2 [ER,M]

ACKNOWLEDGMENTS

We thank Stew Levin for his efforts in helping to organize our research seminar during his visit at SEP, for helping to unload, sort and preprocess the data, and for his many valuable suggestions during our brainstorming sessions. We also acknowledge valued seminar contributions from Bob Clapp and Yetmen Wang that helped illuminate problems related to the Mobil data, but do not appear explicitly in this paper. We commend Mobil Oil for releasing this AVO data set, and thank Bob Keys for traveling out to visit us and discuss the relevant issues. Thorbjørn Rekdal's postdoctorate at SEP was partially funded by Norsk Hydro and the Norwegian Research Council.

REFERENCES

Aki, K., and Richards, P. G., 1980, Quantitative seismology : Theory and methods: W. H. Freeman and Co., New York.

Bleistein, N., 1987, On the imaging of reflectors in the earth: Geophysics, **52**, no. 7, 931–942.

Carvalho, P. M., Weglein, A. B., and Stolt, R. H., 1991, Examples of a nonlinear inversion method based on the T matrix of scattering theory: Application to multiple suppression: 61st Annual Internat. Mtg., Soc. Expl. Geophys., Expanded Abstracts, 1319–1322.

Foster, D. J., and Mosher, C. C., 1992, Suppression of multiple reflections using the Radon transform: Geophysics, **57**, no. 3, 386–395.

Hampson, D., 1986, Inverse velocity stacking for multiple elimination: 56th Annual Internat. Mtg., Soc. Expl. Geophys., Expanded Abstracts, Session:S6.7.

Lumley, D., Nichols, D., and Rekdal, T., 1994, Amplitude-preserved multiple suppression: Stanford Exploration Project Report, **82**, 25–46.

Lumley, D. E., Nichols, D., and Rekdal, T., 1995, Amplitude-preserved multiple suppression: 65th Ann. Internat. Meeting, Soc. Expl. Geophys., Expanded Abstracts, submitted.

Lumley, D. E., 1989, Kirchhoff prestack depth migration: Imaging conditions and amplitude recovery: 59th Annual Internat. Mtg., Soc. Expl. Geophys., Expanded Abstracts, 1336–1339.

Lumley, D. E., 1993a, Angle-dependent reflectivity estimation: 63rd Ann. Internat. Meeting, Soc. Expl. Geophys., Expanded Abstracts, 746–747.

Lumley, D. E., 1993b, Kirchhoff prestack impedance inversion: A gas reservoir pilot study: Stanford Exploration Project Report, **77**, 211–230.

Taner, M. T., and Koehler, F., 1981, Surface consistent corrections: Geophysics, **46**, no. 1, 17–22.

Verschuur, D. J., Berkhout, A. J., and Wapenaar, C. P. A., 1992, Adaptive surface-related multiple elimination: Geophysics, **57**, no. 9, 1166–1177.